Universiteit Utrecht

Climate Physics

Implementing the Lazeroms' Parametrisation of Ice Melt Plumes in a Marine Ice Sheet Model

Master Thesis

Simon Brouwer — 5523583

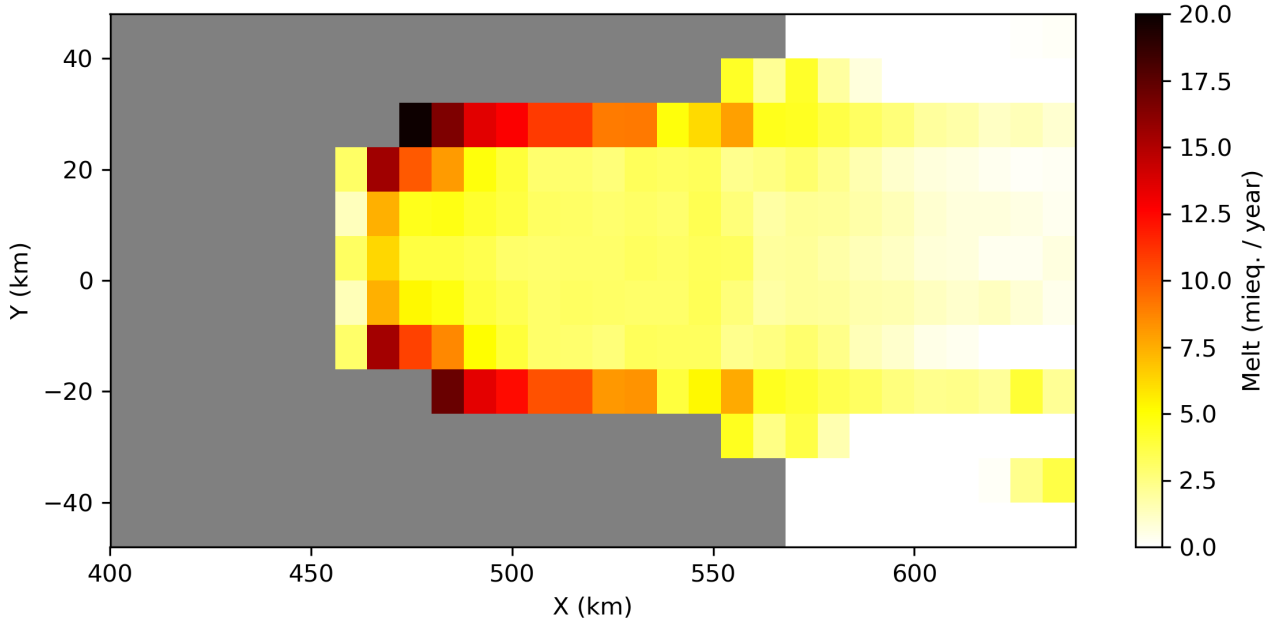

Supervisor:

prof. dr. R.S.W. Van de Wal
H. Goelzer

August 21, 2020

Abstract

In this thesis we look at the implementation of the ice shelf melt plume parametrisation developed by Lazeroms into a hybrid SIA+SSA ice sheet/shelf model IMAU-ICE. To test the melt plume model, we use a the synthetic enbayment setup from the MISMIP+ experiments to observe the behaviour of an buttressed marine ice sheet when it undergoes melt driven retreat. We show the original two-dimensional implementation of Lazeroms causes spurious numerical wiggles irregularities to appear on the ice draft. With modifications to the algorithm we show that the melt plume parametrisation can be effectively used as a tool to determine sub-shelf basal melt without causing irregular ice geometries. However we only show that the parametrisation works in this idealised test setup, we strongly suggest that more work needs to be done to evaluate the plume parametrisation in more realistic setups.

Contents

1. Introduction

In recent years the interest to more accurately model the interaction between marine ice sheets and the underlaying ocean has grown (Favier et al. 2019; Levermann et al. 2020). In part this is due to the recognition that many of the outflow glaciers and shelves on the western side of Antarctica are susceptible to destabilisation and grounding line retreat due to basal melt by a warming Arctic ocean (Parizek et al. 2013). This process, much more than a changing SMB due to climate change, has been a large factor of uncertainty in attempts to estimate Antarctica's contribution to sea level rise (Oppenheimer et al. 2019).

In most model studies where a form of marine basal melt is included, this is mostly done through a simple temperature field driven melt rate or through a parametrised form of reconstructed melt fields based on the observed melt rates of the geometry you are interested in (Beckmann and Goosse 2003; Pollard and DeConto 2012). The reality is however that to the best of our understanding melt is simply not only temperature driven and that using reconstructed melt fields is fine for present day conditions but it serves as a severe limitation if we want to study marine ice sheets in a changing climate.

It is therefore worthwhile to include better melt physics inside our model because this area can be improved. However the actual physics behind sub-shelf melt is complex. When fresh water gets released either at the ice-ocean interface due to temperature driven melt or at the grounding line due to some sub-glacial water stream, this injection of fresh water is often more buoyant then the saltwater environment. This initial volume of fresh water then travels up the ice draft while developing into a turbulent environment interacts both with the ice interface and the surrounding ocean. This plume travels down the ice draft till it has either reached the open ocean surface or when the plume hits a stratified layer which can cause the plume to lose its buoyancy, which means that it detaches from the ice shelf. In both cases the plume will mix out again into its ocean environment (Jenkins 1991).

The development of these plumes is, however, difficult to model, because it requires running a fine ocean model which also contains data about the subshelf geometry. Furthermore, coupling such an ocean model to an ice sheet model to get an ice draft which has a dynamic feedback between geometry and melt is a very computationally expensive and is often an unavailable resource for modellers.

A way forward is to use the one-dimensional melt plume model of ibid. which has been further simplified by Lazeroms et al. 2018 through a parametrisation of its ODE's. Our goal in this thesis is to take the parametrisation made in Lazeroms et al. 2019 and implement and improve upon it. The reason why we think we can improve upon it, is because in the original paper a very basic extension for the parametrisation to two-dimensional space was done: Lazeroms suggested a very simple mapping which transferred two-dimensional plumes to a one-dimensional parameter space; however, this mapping function was not tested by Lazeroms inside a model with dynamic feedback between the plume model and the shelf geometry.

2. UPP Model Description

The melt plume parametrisation is derived from a set of ordinary differential equations describing the growth of a plume of buoyant meltwater under the ice draft and how, as it grows and extends towards the surface, creates a melt rate distribution underneath the ice shelf. This original set of ODE's was described and evaluated by Jenkins 1991; In essence this set of ODE's describes a one-dimensional melt plume which originates from the ice shelf's grounding line. Equation (1) describes how the plume's velocity (U), thickness (D), temperature (T) and salinity (S) develop along-side the ice draft as a function of distance from the grounding line X. Variables with a 'b' subscript, e.g., T_b denote the temperature at the ice-ocean interface whilst the ones with an 'a' subscript indicate ambient ocean properties. Finally, θ indicates the ice draft slope alongside the plume path. Note that the equations describe a stable state and it is therefore an implicit assumption that the adjustment time of the plume is far shorter than that of the shelf's response.

$$\frac{\partial(UD)}{\partial x} = \dot{e} + \dot{m}, \tag{1a}$$

$$\frac{\partial(U^2D)}{\partial x} = D\frac{\Delta\rho}{\rho_0}g\sin\theta - C_dU^2, \tag{1b}$$

$$\frac{\partial(TUD)}{\partial x} = T_a\dot{e} + T_b\dot{m} - C_d^{1/2}\Gamma_T U(T - T_b), \tag{1c}$$

$$\frac{\partial(SUD)}{\partial x} = S_a\dot{e} + S_b\dot{m} - C_d^{1/2}\Gamma_S U(S - S_b). \tag{1d}$$

Important parameters and constants in eq. (1) are the entrainment rate $\dot{e}$ and the meltwater production rate $\dot{m}$, $\Delta\rho$ buoyancy of the plume with respect to ocean environment, gravitational acceleration g, the turbulent drag coefficient C_d and the turbulent exchange coefficients for temperature and salinity $C_d^{1/2}\Gamma_T$ and $C_d^{1/2}\Gamma_S$.[1] A schematic overview of the plume and its quantities we have displayed in fig. 1a.

To create a closed set of equations Jenkins used a linear relationship for the entrainment rate as function of local slope in the form:

$$\dot{e} = E_0 U\sin\theta,$$

where E_0 is a dimensionless scaling constant. This equation effectively indicates that entrainment grows as a function of velocity and that the plume cannot entrain when the ice draft slope is a flat surface.

For the equation of state describing plume buoyancy Jenkins used a linearised variant

$$\frac{\Delta\rho}{\rho_0} = \beta_S(S_a - S) - \beta_T(T_a - T),$$

where the constants β_S is the haline contraction coefficient and β_T is the thermal expansion coefficient.

[1] Values for all constant and other parameters are given in a table found in the appendix.

The final properties needed to create a closed problem are the boundary conditions at the ice-ocean interface. In this case, two are required:

$$C_d^{1/2}\Gamma_T U(T - T_b) = \dot{m}\left(\frac{L}{c_w} + \frac{c_i}{c_w}(T_b - T_i)\right), \tag{2a}$$

$$T_f = \lambda_1 S + \lambda_2 + \lambda_3 z_b. \tag{2b}$$

Here eq. (2a) is the balance equation which describes how the melt fluxes are balanced at the ice-ocean interface and eq. (2b) described the linearised relationship of the freezing point temperature T_f at the ice draft as dependent upon environmental salinity (S), local depth (z_b) and with scaling denoted by these λ coefficients.

With these boundary conditions and the system of equations in eq. (1) we can use a numerical solver in conjunction with a given ice shelf geometry to find the solution to the plume properties and therefore also the melt rate along the ice draft. However, solving these equations inside a model at each time step is a computational intensive process and is too costly to do on any large scale.

2.1. Parametrisation of UPP

A solution proposed by Lazeroms et al. 2018 and Lazeroms et al. 2019 is to use a parametrisation of the ODE's of Jenkins. This is possible because most ice draft configurations lead to a melt rate which shows a certain self similarity which can be used to construct a melt parametrisation which does not require us to iteratively find a solution to a set of ODE's.

Lazeroms in these two papers proposes two different methods to describe the basal melt with a parametrisation. In the first he used a 11th order polynomial to express the self similarity which melt curves seem to share; however, this method is quite error prone and inside a later addendum up to the fifth digit of this polynomial was given so as to get similar results to the ones found in the first paper. In the latter paper (ibid.) this problem was solved by proposing a semi-analytical description of the self similar part. This implementation is not only less error-prone, but is also more elegant to implement.

This melt parametrisation we write as:

$$\dot{m} = \alpha \mathcal{Q}(\theta, T_a, S_a) M(\hat{X}), \tag{3}$$

where we have split the parametrisation into α, a tuning parameter, $\mathcal{Q}$ the melt amplification factor and $M(\hat{X})$ the self-similar melt curve, which we have plotted in fig. 1b. This curve is dependent on a single non-dimensional distance factor $\hat{X}$ which is given by the formula

$$\hat{X} = \frac{(z_b - z_{gl})\lambda_3}{T_a - T_f(S_a, z_{gl})}\left[1 + C_\epsilon\left(\frac{E_0 \sin\theta}{C_d^{1/2}\Gamma_{TS} + c_\tau + E_0 \sin\theta}\right)\right]. \tag{4}$$

Here $\hat{X}$ is primarily dependent on the depth of the grounding line z_{gl}, ice draft depth z_b, ambient sub-shelf ocean temperature T_a and the adjusted freezing point T_f. Furthermore there is a weak dependence of $\hat{X}$ on the local slope, however this contribution is relatively small and has little

impact therefore on determining $\hat{X}$. Finally the melt curve function is given by:

$$M(\hat{X}) = \frac{\sqrt{2}}{4}\left[3\left(1-\hat{X}\right)^{4/3}-1\right]\left[1-\left(1-\hat{X}\right)^{4/3}\right]^{1/2} \tag{5}$$

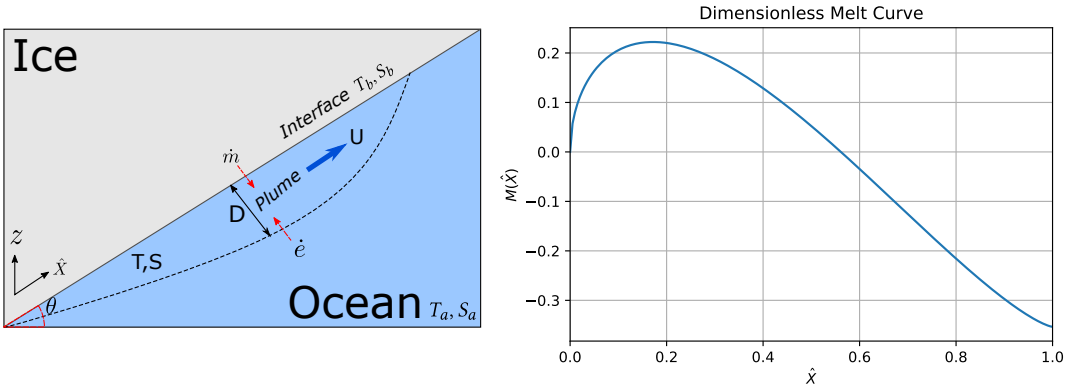

(a) (b)

Figure 1: (a) Schematic overview of the plume quantities involved in defining the plume. (b) Dimensionless melt curve in the melt parametrisation as dependent upon the rescaled $\hat{X}$ coordinate as given by eq. (5). $\hat{X} = 0$ corresponds to the grounding line and $\hat{X} = 1$ is the location at the far field near the shelf edge. Vertical axis is unitless, but defines the sign of the melt and contains part of the non-linear plume response as it develops a turbulent boundary layer travelling down the ice draft slope.

From fig. 1b, the definition of the dimensionless X coordinate and certain assumptions about the behaviour of melt plumes we can deduce a few properties of the melt. (1) It is an *a priori* assumption that a plume can only travel upward; this means that $z_{gl} \leq z_b$ along the melt path and that nominator in eq. (4) is always positive or zero. (2) Valid values for the denominator can only be positive this means that melt can only happen when the local ocean temperature is higher than the freezing point temperature at the sheet-shelf base, i.e., $T_a > T_f$. (3) The difference between grounding line depth and ice draft is the main determining factor for the location on the dimensionless melt curve; whilst the difference between ambient ocean and grounding line freezing temperature determines how much compacted the curve becomes, i.e., the warmer the ocean, the more spread out the melt curve and vice versa. (4) There is only a weak dependence of the melt curve shape on the ice draft slope; as the terms involved are all much smaller than one.

Finally we have the melt amplification factor in this parametrisation $\mathcal{Q}$ which is expressed as:

$$\mathcal{Q} = \sqrt{\frac{\beta_S S_a g}{\lambda_3 (L/c)^3}\left(\frac{1-c_{p1}C_d^{1/2}\Gamma_{TS}}{C_d + E_0\sin\theta}\right)\left(\frac{C_d^{1/2}\Gamma_{TS}E_0\sin\theta}{C_d^{1/2}\Gamma_{TS}+c_\tau+E_0\sin\theta}\right)^3}\left(T_a - T_{f,zgl}\right)^3. \tag{6}$$

We here see that the actual strength of the melt is determined by the local slope which the plume experiences and the melt temperature available when we compare local ocean temperatures to

the freezing point temperature at the grounding line. As before, a table with entries to all the constants can be found in the appendix.

A short note on the tuning parameter α, inside this thesis we have treated α as being equal to 1. We did this because we had no interest in tuning our model runs to get close to each other in providing similar results; however, in applications where you want to tune the melt to observed melt it is handy to denote where the tuning parameter comes into play and that we do not tune the model by changing one of the given constants, e.g., the entrainment rate E, but by way of a multiplicative factor to the calculated melt rate.

3. Extension to 2D

The previous set of ODE's and parametrisation of this equation were derived for a one-dimensional plume, however if we want to apply this melt model to two-dimensional ice sheet models and not just flow line models, we need to determine an extension to the parametrisation which makes it applicable to two-dimensional models.

Such an extension to two dimensions is possible though how this can be done has no definite answer. For the parametrisation to work in 2D we need to determine appropriate one-dimensional projections for the grounding line depth (z_{gl}) and local slope (θ) at every point under the shelf.

Lazeroms presented in his paper a way to do this, however there are also different methods available to find local slope and grounding line depth. In this section we cover different methods we used to calculate the required fields for the melt parametrisation.

In the end out goal is to outline and test different two-dimensional setups with the plume parametrisation to see whether we can apply plume melt in configuration where there is active feedback between shelf geometry and melt rate. We deem a method successful if it is able to describe basal melt without causing the ice geometry to destabilise due to numerical errors.

3.1. Lazeroms Method

The method described in Lazeroms et al. 2019 consists of generating a one-dimensional mapping of a two-dimensional parameter space. We do this through casting multiple plumes and then averaging out their properties to find the local slope and grounding line depth which is applicable for our two-dimensional melt calculation. Lazeroms method starts by looking from a certain point under the shelf in sixteen fixed directions.

For each plume the following immediate check is done: we need to be sure that the direction the plume is originating from is sloped downwards, i.e., that the plume did not need to sink to reach the current sub-shelf point. To do this check we calculate the upstream derivative looking from the downstream point this derivative is used as the local slope associated with this specific plume and we demand as a criterion that this slope must be greater than zero. If not, we reject this plume and continue with the other possible plumes. If, however, the plume does lope downwards to a grounding line, we continue processing the plume with the algorithm.

The next step consists of back tracing along the plume direction till we either find a grounded ice point or we find the outer limits of our domain. In the latter case we again reject the plume,

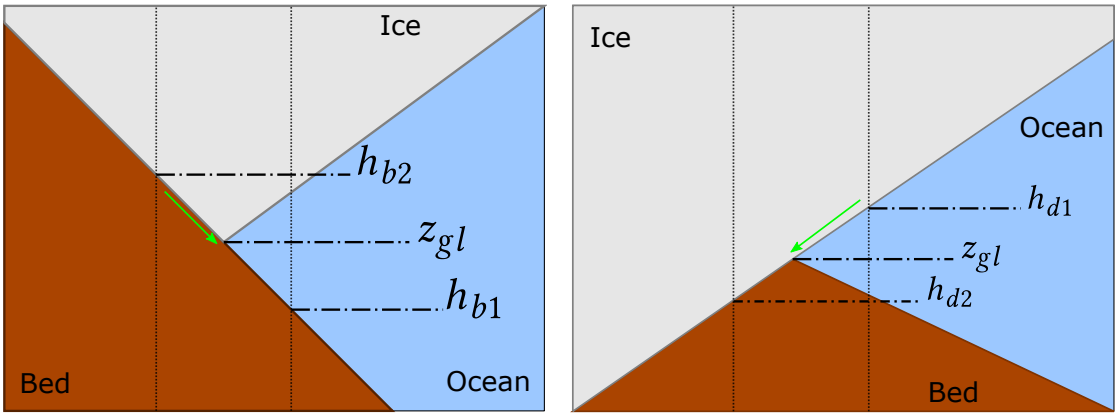

Figure 2: Schematic sketch of the two configurations of grounding line point and how we interpolate using the default Lazeroms scheme to find the position of the grounding line point in between the first floating and last grounded ice sheet point.

in the previous one we take the height of the bedrock of this last grounded ice sheet point to which the plume backtraced. Note this found value is not yet the grounding point depth.

A final important step in this part of the plume model, is to interpolate the final position of the grounding line. We do this because the grid discretisation causes the true position of the grounding line to lie somewhere in between the last grounded-ice point and the first floating-ice point. The interpolation algorithm uses either one of these different methods to interpolate the grounding line position

We interpolate along the bed if the ice draft of the first floating point lies deeper than the bed position of the last grounded-ice point using a linear interpolation formula where:

$$z_{gl} = \frac{1}{2}\left(h_{b,gl} + h_{b,gl+1}\right).$$

For points where the opposite is true, i.e., the first floating-ice point lies higher than the last grounded-ice point; we do a linear interpolation along the ice draft in the following manner:

$$z_{gl} = \frac{1}{2}\left(h_{d,gl} + h_{d,gl+1}\right).$$

The specific geometric configuration of the grounding line associated with each case, we have shown in fig. 2.

As a final check we need to determine if the interpolated grounding line is further below sea level than the initial ice draft point from which the plume was traced. If not, we reject this plume, otherwise we accept the plume.

When all sixteen direction have been traced we simply average them with equal weights where we only average over the *valid* directions. If no valid directions were found we set the grounding line depth to the local ice draft depth and the local slope to zero, this equivalent to

setting the melt at this shelf point to zero.

$$z_{gl}(x, y) = \frac{1}{N_{\text{valid}}(x, y)} \sum_{\text{validn}} z_{n,gl}(x, y), \tag{7a}$$

$$\theta(x, y) = \frac{1}{N_{\text{valid}}(x, y)} \sum_{\text{validn}} \theta_n(x, y). \tag{7b}$$

This is the algorithm as was presented in Lazeroms et al. 2019, however, when we implemented this algorithm as is, we noticed some major shortcomings. We had found that taking only sixteen plume directions to get a one-dimensional projection of a two-dimensional problem is in practise quite coarse and carried with it a number of numerical artefacts due to poor sampling. To generate smoother grounding line and local slope fields, the first extension we made is to go from a sixteen plume average to a N plume one. In section 5 we cover in more detail the problems we identified and how our solutions impacted the results.

3.2. Full Path Tracing

To get to a parametrisation that can calculate the parameter average of N plumes, we need to make an extension upon how the plume paths were traced. In section 3.1 we recursively stepped into sixteen different directions to see whether the paths allowed for valid plumes. The great benefit of only using sixteen directions is that it enables us to simply pass through the grid at regular intervals of Δx and Δy in grid index coordinates. When we have N possible plumes we cannot use this stepping algorithm.

We instead use the Bresenham algorithm (Bresenham 1965) which determines the best way to discretise a line on a finite grid where the line's deviation from the continuous 'real' line is kept at a minimum. See appendix B for an explanation of this algorithm.

The validation criterion stays very much the same, i.e., local slope of a plume at grid point must always be directed downward in the direction of the plume origin. We also keep the rule that if no valid slopes are found that we pick the parameters in such a way that local melt is guaranteed to be zero.

Besides tweaking how many plumes we take into account, there is also some liberty to be taken with how both the grounding line is interpolated and how local slope is determined. In section 3.1 we explained that grounding line is interpolated along either ice draft or bed to a halfway point and that local slope of the ice draft is simply the one-sided derivative coming from the grounding line position. However we can present some alternatives.

3.2.1. Floatation Interpolation of the Grounding Line

For the grounding line, the interpolation can be improved by instead of looking for a halfway point, we can use a linear interpolation using the floatation criterion. (We follow a similar setup as in Gladstone et al. 2010 eq. 9.). We start by looking at the first grounded grid point and first floating shelf point from which the plume originates. We know that ice must start floating somewhere in between these two points. We can denote this fractional position as:

$$\lambda_{gl} = \frac{x_{gl} - x_{sheet}}{\Delta X}.$$

We also use the following equation of state, which says that ice thickness and bedrock depth below sealevel can be interpolated in the following manner:

$$\rho_i H_i(\lambda_{gl}) = -\rho_w H_b(\lambda_{gl}), \tag{8a}$$

$$H_i(\lambda_{gl}) = H_{i,\text{sheet}}\left(1 - \lambda_{gl}\right) + H_{i,\text{shelf}}\lambda_{gl}, \tag{8b}$$

$$H_b(\lambda_{gl}) = H_{b,\text{sheet}}\left(1 - \lambda_{gl}\right) + H_{b,\text{shelf}}\lambda_{gl}. \tag{8c}$$

The subscripts indicate whether the value is taken as the last grounded or first floating grid point. We can now combine and rearrange eq. (8) to yield an expression for λ_{gl}.

$$\lambda_{gl} = \frac{\rho_i H_{i,\text{sheet}} + \rho_w H_{b,\text{sheet}}}{\rho_i \left(H_{i,\text{sheet}} - H_{i,\text{shelf}}\right) + \rho_w \left(H_{b,\text{sheet}} - H_{b,\text{shelf}}\right)}. \tag{9}$$

With this fractional position we can then either interpolate along the ice draft or bedrock to find the ice draft at the subgrid grounding line position. The criterion for choosing which interpolation to do are the same as with the base Lazeroms method described in section 3.1.

3.2.2. Slope Calculation

The other possible part of the algorithm we can modify, is the calculation of the local slope. In the algorithm as proposed by Lazeroms et al. 2018 one-sided derivatives were used, however both higher-order and differently orientated derivatives can be used. The reason why we want to change this derivative, is because the local slope field is rather coarse and tends to exacerbate irregularities inside the ice draft geometry.

We therefore try out in this thesis four different methods for calculating local slope for each plume: (1) downstream one-sided derivatives, (2) central-derivatives, (3) higher-order central derivatives and (4) 'Mean least square' polynomial gradient to see whether an improvement can be made to the smoothness of the local slope fields.

Methods 1 and 2 are simple and use standard numerical definitions. Method 3 uses central gradients where also grid points at distance $i = \pm 2$ are taken into account. Here we follow the method presented in Fornberg 1988 to calculate the appropriate weights for this scheme to find:

$$\delta H_{d,\mathbf{e}_i} = \frac{1}{12}\left(H_{d,\mathbf{e}_i-2i} - 8H_{d,\mathbf{e}_i-i} + 8H_{d,\mathbf{e}_i+i} - H_{d,\mathbf{e}_i+2i}\right), \tag{10}$$

where we have taken the derivative in the direction $\mathbf{e}_i$. Note for all these algorithms that because the plumes can also side-step we need to calculate this difference also for directions which step in both directions. Numerically we do this by stepping concurrently in two directions and then in the slope calculation to use Euclidean distance between cells as derivative denominator. So the direction $\mathbf{e}_i$ does not need to be aligned to only the x or y direction but it can also be orientated along the diagonal.

Then we have the final method 4, here we use a 'Mean Least Squares' routine to calculate the x and y gradient of a fitted polynomial. The more detailed mathematics we have described in appendix C; the short version is that the local gradients in this method are stored as part of

a coefficient vector $\vec{c}$. From this we can extract the x and y gradient in the following manner:

$$\frac{\partial H}{\partial x}(x_i, y_i) = c_2(x_i, y_i), \tag{11a}$$

$$\frac{\partial H}{\partial y}(x_i, y_i) = c_3(x_i, y_i). \tag{11b}$$

To then determine the gradient in the direction $\vec{p}$ out of which the plume originates we combine the x and y directional gradient eq. (11) in the following manner:

$$\frac{\partial H}{\partial \vec{p}} = \frac{\partial H}{\partial x}(x_i, y_i)\cos(\theta_p) + \frac{\partial H}{\partial y}(x_i, y_i)\sin(\theta_p), \tag{12}$$

here θ_p is the angle between the first backtraced point and the starting point.

3.3. Reverse-Lagrangian flow

Another completely different take on determining plume path properties is by doing a reverse-Lagrangian simulation of grounding line particles at every shelf grid point. Here the central assumption is that the dominant plume is aligned with the ice velocities inside the ice, this means that backtracing along a flow direction also gives us the orientation and origin of predominate plume which should inform melt parameter properties at the grid point of interest.

To do the Lagrangian backtracing we take the velocity field inside the ice at a time n to calculate the melt at time $n+1$. We next use an Adam-Bashforth scheme to do the Lagrangian advection with the form:

$$\vec{x}_{n+2} = \vec{x}_n - \frac{3}{2}\mathrm{d}t\,\vec{v}_n(\vec{x}_{n+1}) + \frac{1}{2}\mathrm{d}t\,\vec{v}_n(\vec{x}_n) + \vec{N}(\vec{v}_n), \tag{13}$$

here $\mathrm{d}t$ is dynamically determined by looking at the largest possible time step[2] that would not violate the CFL condition at any sub-shelf grid point. Note that unlike the usual Adams-Bashforth method, we do not use a varying velocity, because of our assumption that the development of the plumes is instant when compared to the adjustment time of flow inside the ice. Another important remark is that to get the first advected position, we cannot use the scheme in eq. (13), for the first step we use a simple Euler forward advection scheme.

The final term in eq. (13), $\vec{N}$ is a Brownian motion drift term which causes especially points at shelf areas with low velocity to experience some drift. We do this because in our initial investigation we found that many ice points are backtraced to the same grounding line when you go farther away from the ice shelf grounding line. To artificially smooth out the resulting grounding line depth field and also to incorporate the uncertainty of the plume origin for points which are further away from any grounding line, we have added Brownian motion in the following manner:

$$\vec{x}^b_{n+1} = \vec{x}_{n+1} + 2\vec{U}\sqrt{\frac{3\,|\delta t|\,K}{2}}, \tag{14}$$

where K is the diffusivity and $\vec{U}$ is a uniformly distributed two-dimensional vector sampled from the range $[-0.5, 0.5]$. To incorporate the effect that we are less certain about the origin of

[2] Because we are backtracing the flow time steps are implicitly taken as a negative number.

the plume when we are further away from the shelf, we make the diffusivity K dependent on the local slope under the shelf. The assumption here is that local slope is larger close to the grounding line than it is in the far-away field.

$$K = \frac{K_{\max}}{\sqrt{1 + (\theta/10^{-3})^2}}. \tag{15}$$

At present this slope dependent diffusivity is done in an *ad hoc* fashion where we primarily calibrated the constants and sensitivities in eq. (15) to cause a visible smoothing of the resultant grounding line depth field. Therefore we do not presume that this diffusivity is scaled to some unknown parameter though the addition of Brownian motion was justified by postulating that back tracing shelf ice velocities does not have to correspond to the actual paths the melt plumes take. So we keep in mind that the calibration of the diffusivity is dependent on setup and the desired amount of smoothing and not a detailed analysis of actual melt rates versus model melt rates.

We now run the solver of eq. (13) until we are either in a grid point which the model recognises as being grounded or when we violate any of the plume conditions which we also gave in section 3.1, i.e., local slope must go up from the plume to the grid point. This condition of local slope we calculate by taking the ice draft at the centre grid point and then calculate its gradient with respect to the bi-linearly interpolated ice draft of the first advected point.

Note that while we are backtracing we also mark grid points we pass as being associated with the plume that goes to the position we started from. This is done to later average out multiple plume properties at grid points to give us smoother results.

When we have reached a grounded grid point we again use the interpolation devised by Lazeroms in section 3.1 for grounding line interpolation or the one based on the floatation criterion in section 3.2 to determine the subgrid position of the grounding line. Note that these schemes use the grid values at integer coordinates. So the final and penultimate coordinates of the backtracing scheme are first rounded to their nearest integer positions before these other interpolations are used. The result of this final interpolation is treated as usual and must have a lower position below sea-level than the ice draft point where the backtracing started, otherwise we fix the melt for the coordinate at zero.

A final problem that we can encounter is that plume cannot be backtraced to a grounded ice point within a reasonable amount of time, or melt plume paths which, due to the Brownian motion, escape the model grid. In the interest of model run time, we simply ignore these points and set the melt to zero at the points where this occurs. This does not cause a real problem, because this only happens near the model boundary where melt is usually already negligible.

3.4. Overview

This combination of grounding line, slope algorithms and sub-grid interpolation schemes leaves us with a net sum of 11 configurations. In the next section, section 4 we cover more in depth the specifics of the setup, now we would like to present a table of the possible melt configuration we can combine.

Grounding Line Algorithm	Slope Method	Interpolation Method	Section
Lazeroms' 16 Directions	one-sided	mid point	**section 5.1**
Full Tracing	one-sided	mid point	**section 5.2**
		floatation	-
	central lo	mid point	**section 5.3**
		floatation	-
	central ho	mid point	-
		floatation	-
	MLS	mid point	**section 5.4**
		floatation	-
Lagrangian	one-sided	mid point	**section 5.5**
		floatation	-

Table 1: The evaluated melt setup configurations is this thesis. For explanation of the grounding line algorithms see sections 3.1 to 3.3. The slope methods are highlighted in section 3.2.2 and the difference between mid point and floatation interpolation for the grounding line is explained in section 3.2.1.

In this thesis, however, we shall not present all these combinations one-by-one. Far more helpful is to zoom on into the most effective setup inside the current model, and highlight other setups' shortcomings with respect to one we found to be the most well performing.

As we show in section 5 and later discuss, the full tracing method with central, higher order slope gradient calculation gives the best results in this model setup. We try to make this case by contrasting certain options, e.g., the slope method, and show why central gradients can be seen as an improvement over the default one-sided gradients employed in the original algorithm.

Certain experiment names in table 1 we have printed in bold. These are the experiments we are going to present in section 5, the way in which we are going to present these results is mainly by building up to the full-tracing, central derivatives method, starting from the original Lazeroms algorithm and iteratively show how we changed this and the subsequent effect this change then had on the model output results.

4. Test Setup to Evaluate Model Melt

4.1. Model

We run and test these setups with IMAU-ICE, a hybrid SIA+SSA model where the simplified SIA and SSA approximations are solved separately from each other on a regular grid and combined together as the ice velocity when updating the ice thickness. We furthermore run this model on a lower resolution grid (8 km by 8 km) which enables us to do experiments on a mesoscale temporal range within a reasonable time frame.

Note that because we run this model on a regular, lower resolution grid we have problems to accurately resolve the point at which grounded ice becomes a floating shelf. We call this exact position the grounding line. This leads to the problem detailed in Pattyn et al. 2012 were it is shown that during a marine ice sheet retreat scenario the unresolved grounding line responds

inadequately which disallows the marine ice sheet to retreat. We therefore use the solution which Schoof 2007 proposed and which is also implemented in Pollard and DeConto 2012 where we resolve the position of the grounding line on a subgrid scale and use ice flow continuity equation there to more accurately resolve the ice flux across the grounding line.

Inside the model we describe the deviatoric stresses τ_{ij} inside the ice through strain rates D_{ij} by using Glen's flow law in the following manner:

$$\tau_{ij} = A^{-1/n} D_e^{\frac{1}{n-1}} D_{ij}, \tag{16}$$

where D_e is the second scalar invariant of the strain rate. At the bottom we use a Weertman-type sliding law for basal frication inside our experiments which is given by the formula:

$$\tau_b = -\left(\rho_i g H_i \beta^{-2}\right)^{\frac{1}{m}} |\nabla h_s|^2 \tag{17}$$

at all grounded grid points.

Further important assumptions are that the ice is isothermal and thermostatic;[3] so we have no evolution of the temperature due to friction and basal heating inside the ice. We also simplify basal sliding by applying a Weertman-type sliding law at all grounded points and the rheology of ice we prescribe for the whole ice mass with one uniform value which we use as a tuning parameter to get to our initial state which we have described in section 4.2.

4.2. Test Geometry

The setups within the model are then evaluated in a MISMIP+-like setup. The MISMIP+ setup, like the other MISMIP experiments, allow for more sensible model intercomparison studies by focussing in on specific mechanics inside an ice model. The MISMIP+ setup is especially useful for us, because the geometry is designed to test the ice model's capabilities to simulate the effect of melt on embayment area with an ice shelf that experiences strong buttresing effects from the two banked areas and also rests on a retrograde slope. In fig. 3d we show the importance of this side wall buttressing in our final model setup. We see here the effect buttressing has on impeding ice flow for floating ice. The bright red colours correspond the floating ice that is completely buttressed.

The geometry of the MISMIP+ is bounded inside the x domain in between 0 and 640 km and in between −40 and +40 km in the y domain. The original larger setup was first described by Gudmundsson 2013. We also ignore bedrock adjustment to due the presence of the ice mass. The geometry we describe in the following manner:

$$z_b(x, y) = \max\left[B_x(x) + B_y(y), z_{b,\text{deep}}\right], \tag{18a}$$

$$\tilde{x} = x/\bar{x}, \tag{18b}$$

$$B_x(x) = B_0 + B_2\tilde{x}^2 + B_4\tilde{x}^4 + B_6\tilde{x}^6, \tag{18c}$$

$$B_y(y) = \frac{d_c}{1 + \mathrm{e}^{-2(y-w_c)/f_c}} + \frac{d_c}{1 + \mathrm{e}^{2(y+w_c)/f_c}}. \tag{18d}$$

[3] Ice temperature is set to 263.2 K everywhere.

In fig. 3a we have given a plot of eq. (18c) where we have applied the condition that the depth of the bedrock is not allowed to drop below −720 m. Note that from $x = 350$ km to $x = 500$ km the central flow line contains a retrograde slope. Also note the steep side walls in fig. 3b which cause the strong buttressing of the floating ice inside the enbayment area. The resulting geometry given by eq. (18a) we have shown in fig. 3c

Additional boundary conditions which are applied in this setup is that at the top and bottom y boundary there is a free slip condition being applied. At the left x boundary we apply a no-slip condition and at the ice front on the right side of the domain we have unrestricted outflow, simulating the presence of a calving front.

We first run this model with a resolution of $\Delta x = \Delta y = 8$ km without any melt to a stable state. Like in the MISMIP+ paper we require that a stable state be found where the grounding line rests at 450 km from the left model border. To find this stable state we tweak the ice rheology parameter till we have a configuration which has this stable grounding line position. In figure fig. 4 we show the final stable velocity magnitude and the shape of the ice sheet/shelf along the central flow line inside the model.[4]

In subsequent runs which use this initial ice geometry as a starting point, all the ice parameters will stay the same. However, for the plume melt to be calculated, we also need to give appropriate values to the ambient ocean temperature and salinity (T_a and S_a in eq. (1)). In this test setup we keep these fields simple by supposing that the ocean inside and around the embayment is isothermal and isohaline. We define two types of oceans, i.e., a warm and a cold ocean. Most of the times we only evaluate the warm ocean, but at certain times we also want to study the model's behaviour when a lesser melt forcing is applied.

	Warm	Cold
Temperature	−1.0 °C	−2.0 °C
Salinity	34.6 PSU	

Table 2: Ambient ocean properties inside the model during the runs where melt is being calculated with the plume model.

Also note that we assume that there is no salt inside the ice draft's melt fluxes, i.e., $S_b = 0$.

[4]We refer to the appendix for the used rheology parameter.

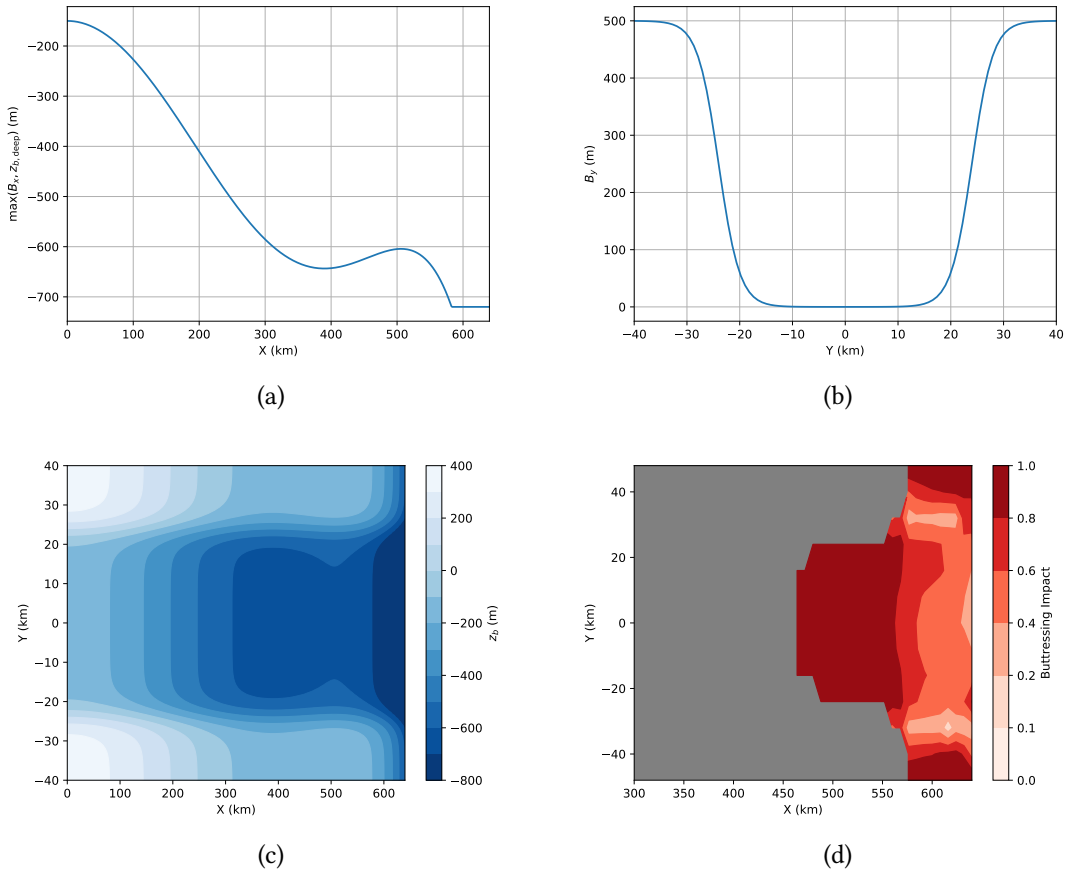

Figure 3: The MISMIP+ bedrock geometry. (a) The function $B(x)$ show casing the bedrock profile along the central section of the domain. (b) The shape of the side walls given by the function $B(y)$, (c) the shape of the computational domain and (d) the relative importance of the effect of ice buttressing inside the embayment area for floating ice. The unit is dimensionless, with 0 corresponding to an free floating ice shelf and 1 to a fully impeded ice shelf.

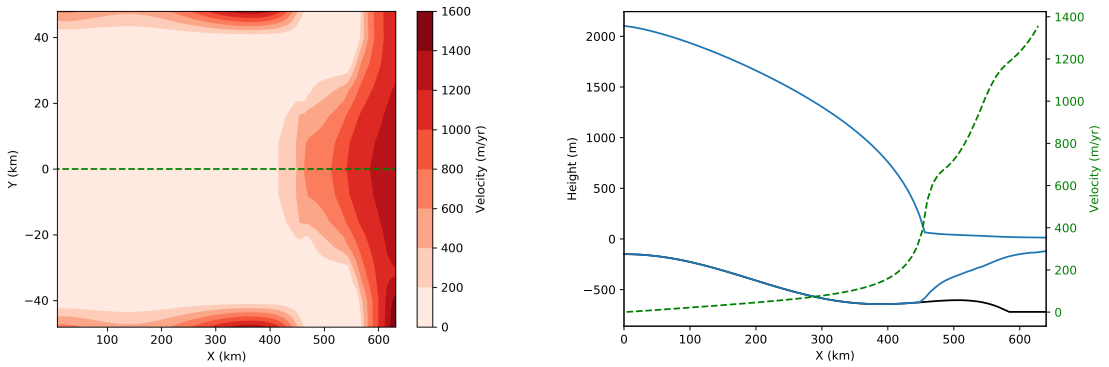

(a) (b)

Figure 4: (a) The velocity magnitude in the model after a stable state was achieved with central flow line (dashed green line) plotted. (b) The ice geometry and velocity along the central flow line inside the enbayment.

5. Results

5.1. Lazeroms Method

We first present the calculation of the melt parameters (grounding line depth and local slope) and the melt itself for the ice geometry after it had reached a stable state. In fig. 5 we show these fields. In these pictures the grey areas indicate the presence of a grounded ice sheet. When we look at the grounding line field, we notice that it does not appear to be very smooth. For sure, some irregularities are due to the fact that on a finite grid you always get some artefacts, but this roughness seems to be a result of the method we use to determine to this field, because if we now look at the slope field we see similar patterns.

This roughness can have significant effects on the melt rate calculation, because the melt rate response is highly non linear, a good example of this is how the dimensionless melt curve responds non-linearly to a linear growth of distance between grounding line and ice draft. This means that the melt rate which we have obtained in fig. 5 may distort the ice draft with noise and that noisy pattern which is now transferred to the shelf geometry will then undergo more amplification when we redo the plume path calculations.

Also note that the melt rates are not the highest at the first point after the grounding line for the furthest inset of the enbayment but a point after that. This is in part caused by the fact that the melt optimum is found some distance away from the grounding line, so we often see that even though slopes are the largest at, or very near the grounding line; the highest amount of melt is found some distance removed from this point.

We test whether we can use this method by running a 1 kyr simulation of the melt-shelf feedback in the MISMIP+ setup to see whether the melt calculated by this algorithm causes a stable retreat of the grounding line. As can be seen in fig. 6a the shelf geometry at different time slices is irregular near the grounding and the shelf is at many times at the calving thickness

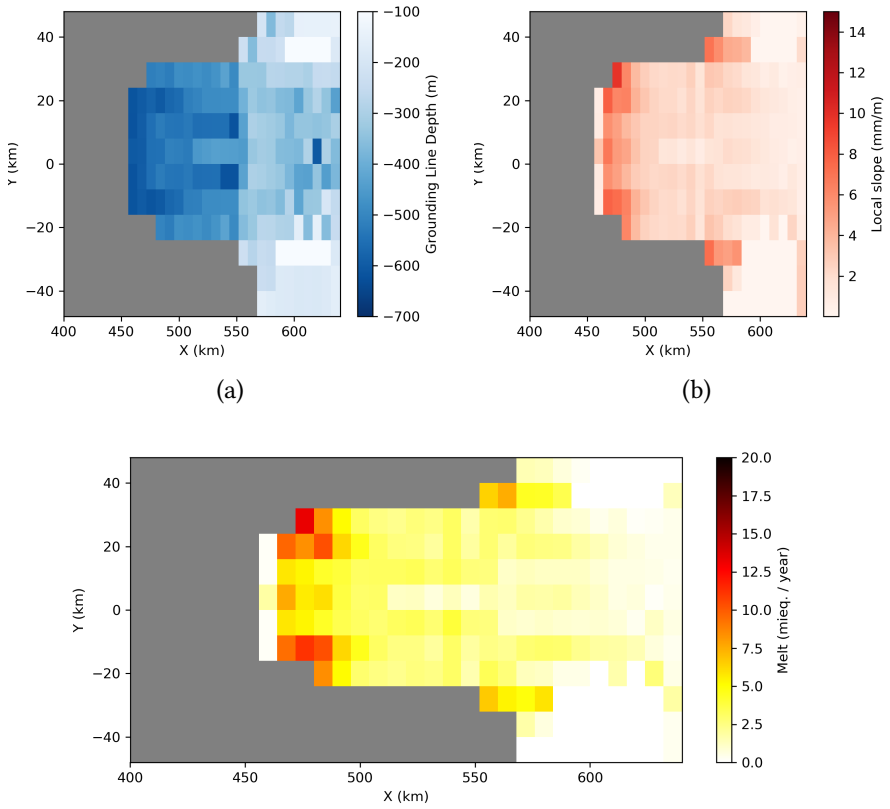

Figure 5: Plume grounding line depth, slope and melt calculation using the original Lazeroms method for the ice geometry after a stable state was reached. Grey colouration indicates a non-shelf grid cell.

criterion inside the model, which we have here represented by the dashed red line. So we observe at a model run's start a very quick, but also non smooth melting of the shelf. Furthermore over time we get these isolated patches of ice which are cut off from the main shelf by being surrounded by ice below the calving thickness. At present we have not yet found a solution to this problem, for we often saw in these enbayment experiments that these holes appeared inside the ice mainly in the horizontal direction, but that there was still a continuous ice bridge extending from the enbayment's sides to the semi-detached ice mass. We opted therefore to let these features remain and let them be an indicator of how melt effects the whole shelf.

However, the quick and irregular dissolving of the shelf may also be due to us applying too dominant a melt rate; to check for irregularities appearing at lower melt rates we use a colder ocean as a melt driver and redo the experiment. In fig. 6b you can again see a few snapshots of the ice geometry. We observe that we still have a spiky melt pattern appearing near the grounding line which causes the sub-shelf geometry to become rough.

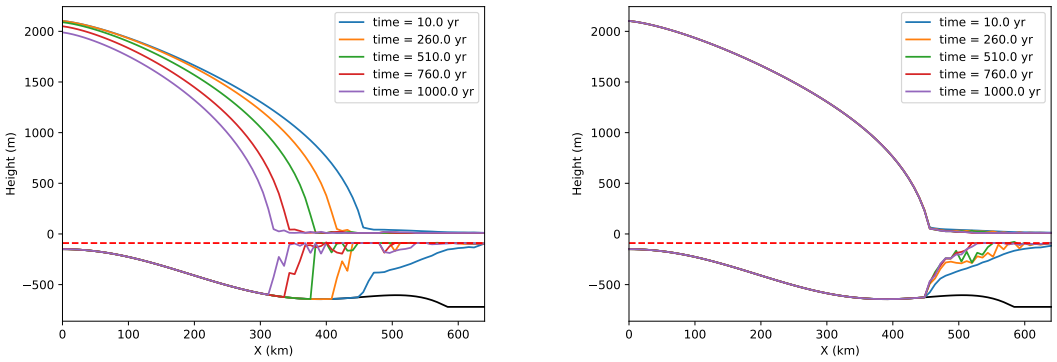

(a) (b)

Figure 6: Geometry slices of the model setup along the central flow line. (See dashed green line in fig. 4.) In (a) we have run the original Lazeroms setup with an isothermal oceanic forcing of −1.0 °C for 1000 years. In (b) we have run the same Lazeroms setup but now with an isothermal oceanic forcing of −2.0 °C.

5.2. Full Tracing Method – One-side Plume Derivatives

One of the important causes of the irregularities which appeared in the grounding line and local slope fields which we discussed in the previous section, is that with the Lazeroms method we have a high chance of undersampling the grounding line. What we mean by this is as follows: with sixteen directions to determine local variables for grounding line and slope we encounter two problems. (1) Because we follow along these sixteen directions to eventually find a plume origin point on the grounding line, the distance in between sampling points steadily increases as we go further away from the point of origin. This is problematic if we have large variations in depth along the grounding line, for a simple shift in point of origin may then mean that we sample the grounding line in a completely different way.

(2) Another difficulty is determining the local slope of a plume. Like we said before, local slope is determined through calculation of the downstream differences looking from the plume direction to the starting point. This means that we use one of the sixteen directions to determine where we sample the grid. However, this is problematic because not all grid step sizes exist on the same stencil. In fig. 7 we see that we have a central square around the point of origin for the first eight directions (grid cells with a solid circle), but that the other eight directions pointers step with a larger footprint (grid cells with a hollow circle). This means that when we calculate the gradients for these final eight directions we do not calculate the gradients on a cell edge of the point of origin, but the gradient somewhere inside the interior grid stencil. What this means is that you get a sampling bias for plumes which have a local steep gradient and this can lead to a melt amplification which due to the shelf-melt feedback leads to further exacerbation of this local steepness. In the end, these one-sided gradients make the melt scheme very sensitive to local saddle points in the ice draft.

The full tracing method we described 3.2 is meant to solve these two issues by not only taking

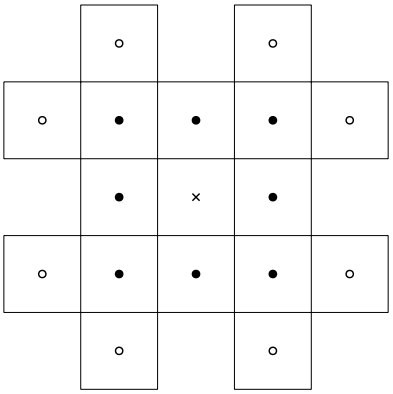

Figure 7: Step and gradient stencil used by Lazeroms method and the full tracing method. The Lazeroms method uses for a single of the sixteen plumes one of either hollow or solid circles as a stepping pattern to backtrace to the grounding line. (See section 3.1.) The full tracing method only uses one of the solid interior grid steps during its backtracing procedure, furthermore it can vary its step direction after each taken back step. (See appendix B.)

into account all valid grounding line points, which solves the undersampeling issue (1) but also by using a grid stepping algorithm which can only step to its eight adjacent neighbours we calculate local slope always on the boundary of the interior cell.

To show how this change has effected the offline calculated grounding line depth and local slope fields, we have followed the same procedure as in section 5.1. If we now compare fig. 8 to fig. 5 we see that the both the grounding line field and the local slope contain a lesser amount of noise and appear smoother. Note also that the grounding line depth inside the main enbayment has not only become more uniform, but it has also deepened for most points inside the enbayment.

Next we look at how the melt feedback effects the ice geometry. In fig. 9 we can see that the the problem of irregular geometry has actually worsened if we compare it to fig. 6a. We see in the new results that irregularities appear alongside the ice draft and that in the end these spikes become these isolated ice islands. The number but also longevity of these instabilities has increased if we compare the new results to the results of the Lazeroms method in fig. 6a. The reason why with more plumes the result has become more unstable must then be explained as a consequence of using one-sided gradients in the direction of the grounding line.

For with more possible plumes the probability has also increased that you find valid plumes even when the geometry becomes unstable. And this melt stays significant enough that even though ice is essentially a thin film of deformable material that is mainly governed by diffusivity and that inside IMAU-ICE even isolated ice patches experience this diffusivity. The fact that we then get these sustained ice irregularities means that the melt is strong and persistent enough to create the permanent fixtures we observe in fig. 9.

Another important difference with the Lazeroms method is that the grounding line has undergone slightly less of a retreat.

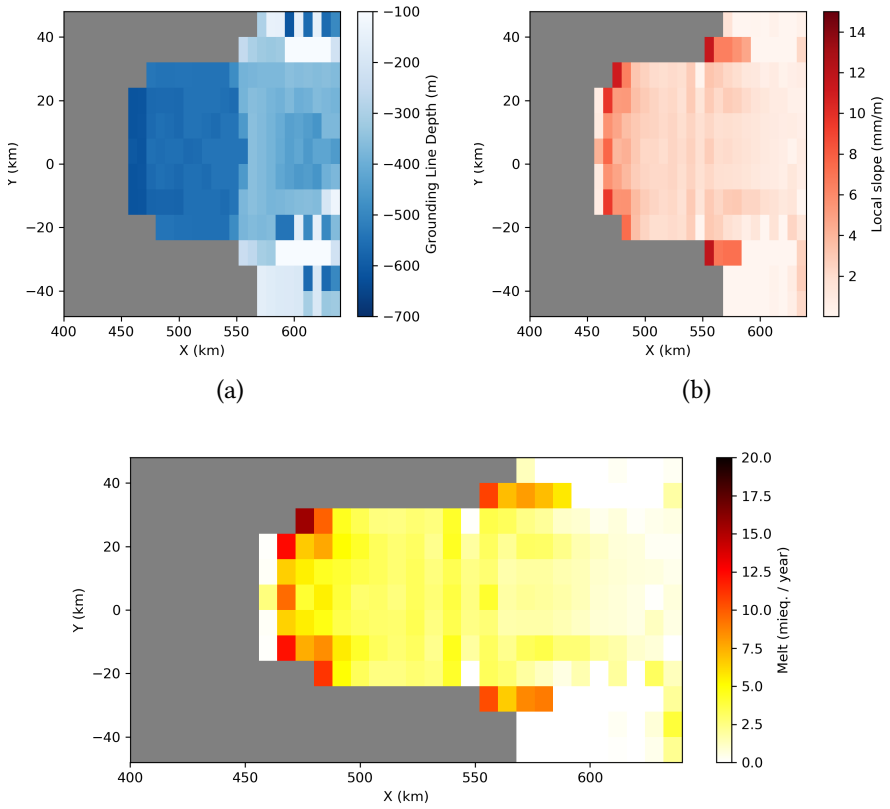

Figure 8: UPP grounding line depth, slope and melt calculation using the full-tracing method with one-sided gradients for the ice geometry after a stable state was reached. Grey colouration indicates a non-shelf grid cell.

5.3. Central Gradients

In section 5.2 we have suggested that using all valid grounding line points and taking only local gradients into account at cell borders would smooth out the variable fields and cause less spikes to appear inside the ice draft. However, in a dynamical application we still have feedback which causes unrealistic behaviour inside the algorithm. A possible reason why this happens is because the parametrisation is not self-dampening. If we turn back to the melt description, we said that only sections of the ice draft which were upwardly sloped from the plume origin were taken as valid melt plumes. A problem with this is that once an ice spike starts to appear as a lowering of the ice, the point to the right of this depression will not experience any melt, because the slope is in the wrong direction. However, the point which is deepening more quickly than the surrounding points will experience melt amplification, for a larger gradient in ice geometry will cause the entrainment and thus the melt to also increase. This means that a steeper slope always leads to more melt which causes the slope to further steepen, i.e., the

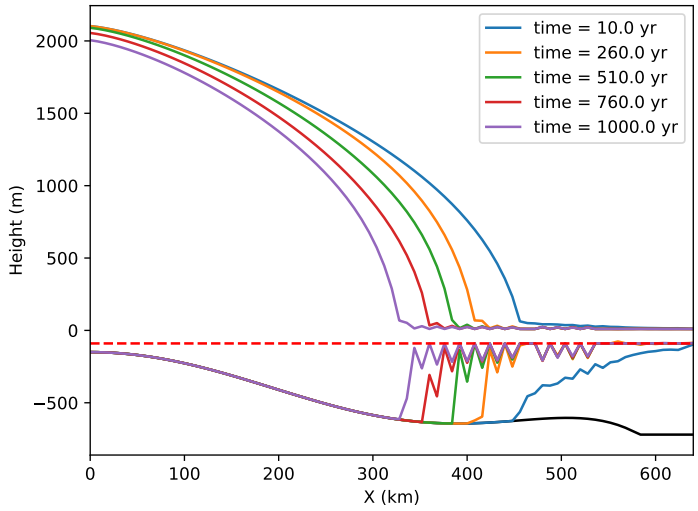

Figure 9: Dynamic feedback response of the full-tracing method with one-sided gradients directed along the plume path from the grounding line outward at different time slices. The model was run for 1 kyr.

entrainment driven melt is essentially a positive feedback loop. We need, therefore, a way to dampen this behaviour of the plume parametrisation as not to lead to a run-away melt effect.

A technical solution we suggest is to use central gradients. The benefit of using central gradients is that these are less sensitive to local saddle points inside the ice draft which is something that would smooth out the melt output. Also, unlike the one-sided gradients which were calculated on the central cell's borders, central gradients are always evaluated at the cell centre. This also means that when we average the individual plumes we average quantities which are defined on the same point instead of at different points along the cell border.

In this section we present the central gradient method with a 3x3 stencil (lower order) and not the higher order central gradient method with a 4x4 stencil. This is done because the higher order stencil cannot be applied too close to the border and with our small domain we would like to include as many possible grid cells. Furthermore, during testing of this larger stencil the increase in accuracy did not lead to significantly different results we had obtained using the smaller central gradients stencil.[5]

We first run the model in an offline fashion and in fig. 10a we have displayed the calculated average local slope of the plumes on a static ice geometry. A notable difference with fig. 8 is that the local slope is much smoother; even when calculated just for the initial ice geometry. Furthermore, when we look at the first floating ice points furthest inside the enbayment we also notice that the local slope with central gradients is not greatly reduced like it was in the case of one-sided derivatives.

Now we run the model with dynamic feedback between melt and geometry. In fig. 10b we

[5]See section 3.2.2 for the central difference weights associated with a 4x4 stencil.

can clearly see that we have practically removed the creation of spurious melt peaks which both appeared in section 5.1 and section 5.2. Furthermore, the problem of isolated ice islands has almost been completely solved because we now have a shelf which monotonically thins to the calving thickness. A problem area which we can still identify in this result is how near the grounding line we have such concentrated melt that at many time slices a local maxima of the ice draft is found close to the grounding line point. This sometimes causes the ice thickness here to be close or even at the calving criterion.

Also note that the amount of grounding line retreat we observe in fig. 10b is different from both the Lazeroms method fig. 6a as the full tracing method with one-sided gradients in fig. 9. This shows that the dynamic interaction between melt and corresponding grounding line retreat is complicated process even within a simple test setup.

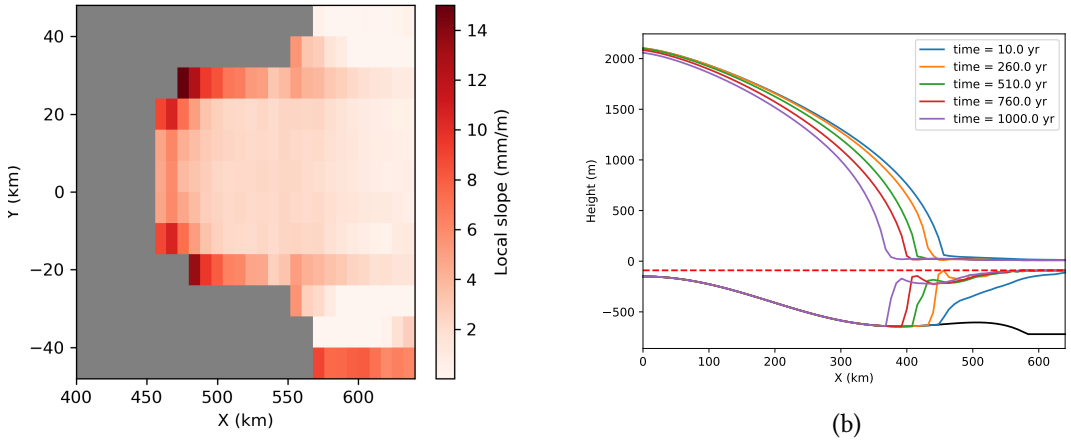

(a) (b)

Figure 10: The results of (a) the local slope calculation of the initial geometry with central gradients and (b) time slices from the model run with the full tracing method and central gradients.

5.3.1. Floatation Criterion

One additional variation we have not yet discussed, is the usage of a different interpolation criterion to find the grounding line. As we had explained in section 3.2.1 we could use a floatation criterion interpolation. Again we look down the central flow line of the model and in fig. 11a we show how the position of the grounding line differs as dependent on these two methods.

We observe that the floatation interpolation in this setup causes a more rapid retreat of the grounding line during most moments, but that retreat behaviour overall is very similar to the to default interpolation scheme.

Besides looking at the position of the grounding line, it is interesting to look at how the total melt has changed by switching interpolation algorithms. On the right of fig. 11 we have

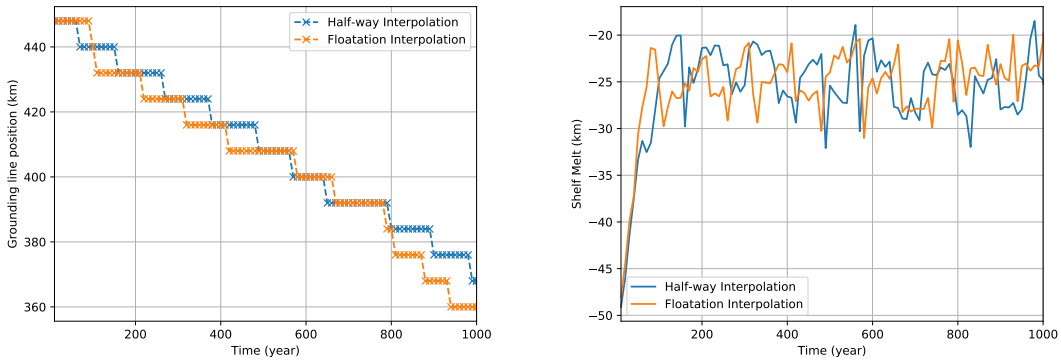

(a) (b)

Figure 11: The position of the grounding line (a) and the total subshelf melt rate (b) for a full tracing with central derivatives setup where either a half-way or floatation interpolation was applied for every plume.

displayed the total melt over the shelf area in Gt/yr. We notice that in general the melt pulses for the floatation scheme happen earlier, but they are not stronger than the melt pulses observed with the halfway method.

5.4. MLS Gradients

Another available option to determining the local gradients is instead of using finite difference on a grid to determine a gradient, we can use a fitted 2nd order polynomial surface to the ice draft to determine the local slope. The benefit as with central gradients is that this method better estimates the gradient at saddle points and it the gradient is also fully localised at the grid cell centre where we want to sample the local slope.

In fig. 12 we have plotted the sideways profile along the central flow line of the ice geometry at different time slices. As we can see the ice draft is far less noisy than with methods using a one-sided gradients. However, the profile does contain more noise than the model run where we used central gradients. A big difference in between the results of this method with the one in fig. 10b is that near the grounding line we do not have a ice cavity inside the shelf.

We also remark upon the fact that the retreat of the grounding line exhibits similar behaviour to what we saw in fig. 10b with a grounding line resting at 350 km along side central flow line.

5.5. Lagrangian Method

The final method we tried out was the Lagrangian reverse flow tracing method. In fig. 13a we show the determined grounding line depth by backtracing points along the shelf velocity after the model was initialised to a stable state geometry. We first note that the field is far more uniform than fig. 5a and also more uniform than the smoother results of fig. 8a. This is because the backtraced plumes are in this setup completely aligned with the flow which

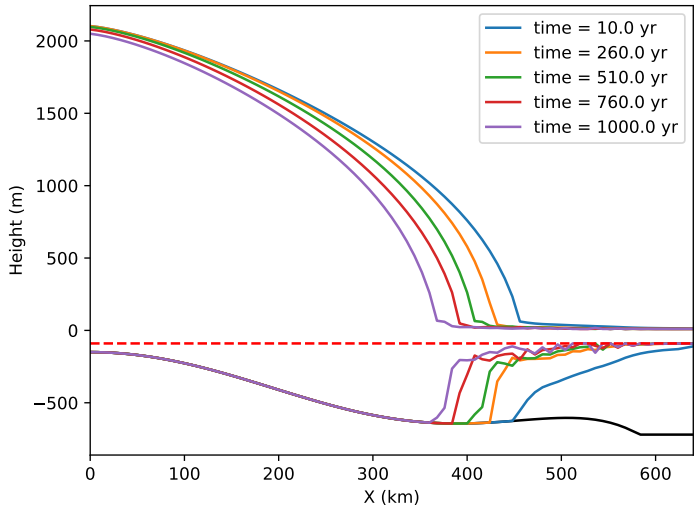

Figure 12: Melt simulation for 1000 years within a −1 °C isothermal ocean with full tracing and MLS gradients.

is predominantly in the horizontal direction. This also means that even shelf points mainly outside the central enbayment area have plumes associated to them which according to the Lagrangian method originated somewhere from the back deep waters of the enbayment area.

Next we run the model with this Lagrangian method. In fig. 13b we see a situation very similar to fig. 9 developing: namely a very irregular retreat of the grounding line with spikes embedded inside the ice draft geometry.

5.6. An Overview

In the previous sections we have presented some of the combinations of algorithms and shown a qualitative analysis of each method on not only the smoothness of the parameter fields at the start of model execution, but also on the stability of the dynamic feedback between melt and shelf geometry. As a final analysis we present in fig. 14 on the left the total melt rates in Gt/yr under the shelf of the discussed methods and on the right for the same set the total mass of ice remaining inside the model.

Here we notice a couple of things. (1) The total observed melt rate of the Lagrangian setup peaks to higher values than all other methods. (2) We have a high amount of initial melt in all setups of around −50 Gt/yr, but after approximately a 100 years the methods tend to a melt rate of −20 Gt/yr. (3) Melt happens with bursts: if we take a closer look at a line, e.g. the red line, then we notice that after a period of lower melt of around −15 Gt/yr we quickly jump up to melt rates of −25 Gt/yr and then we quickly return to period of lesser sustained melt. We suggest this is related to the fact that the shelf structure quickly thins in all cases to the calving thickness. This not only means that there is less ice available, but also that the local ice draft slope has become shallow over the largest part of the shelf, e.g., in fig. 12 we note that after 200

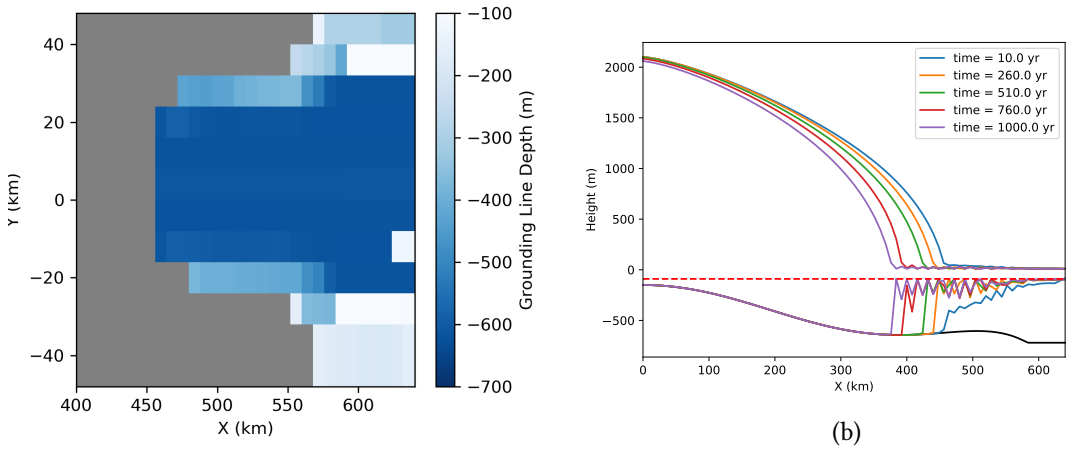

Figure 13: (a) Calculated grounding line depth for the initial stable state geometry after a stable state was reached. (b) Melt simulation for 1000 years within a −1 °C isothermal ocean with Lagrangian backtracing and one-sided gradients.

years we have a steep slope at the grounding line but for the remainder of the shelf this slope quickly flattens out.

If we now look to the total ice mass above floatation we notice mainly that even though the Lagrangian method has higher peak melt rates, that this does not mean that it has a lesser amount of ice inside the model than the central and MLS full-tracing methods. We noticed that with the standard Lazeroms and one-sided full-tracing method we have a far more significant loss of ice. That we can have a higher loss of ice mass but no significant difference in shelf melt, must mean that inside these two runs more of the ice is floating and flowing out of the domain. This we can see in fig. 15a where both these methods are also associated with the quickest retreat of the grounding line. So the increased ice flux at the model's calving front also contributes to loss of ice mass in these two scenario's.

Another important aspect of fig. 15a is that each method we tried also exhibited a different amounts of grounding line retreat over the same amount of time. This is an important property to keep in mind because as we saw in fig. 14 even though similar melt rates are observed for each method, there were differences in observed total ice mass loss. Theses losses are closely related to the patterns observed in fig. 15a, therefore we note that the impact which the basal melt has on grounding line retreat is far larger in terms of sea level rise than when we look at fig. 14a. We also note that outside of central flow line, in fig. 15b, that the final grounding line positions for all methods are vertically aligned at the back of the enbayment. This shows that for even methods with a large noise amount of numerical noise, e.g., the Lazeroms method, the grounding line stills retreats in a stable fashion.

One important aspect of using a model with a coarse resolution where the position of the grounding line cannot be accurately tracked is that we get to the situation we observe in fig. 15a where the retreat does not happen smoothly but in jumps. This erratic retreat of the grounding

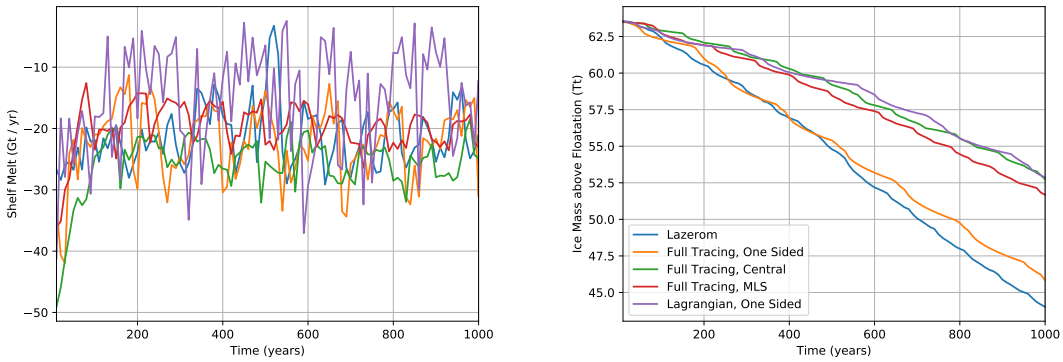

(a) (b)

Figure 14: (a) The total subshelf melt rate in Gt/yr. (b) The total ice mass above floatation inside the model domain in Tt.

line may be part of the reason why the shelf-melt feedback is prone to instabilities because the melt is very dependent on shelf geometry.

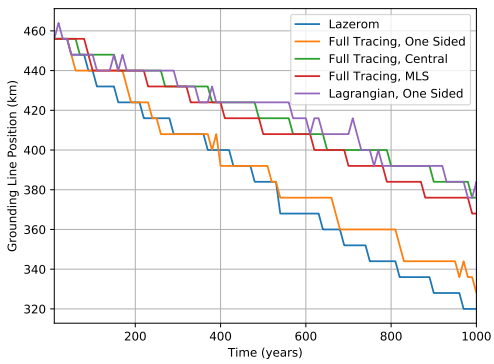

(a)

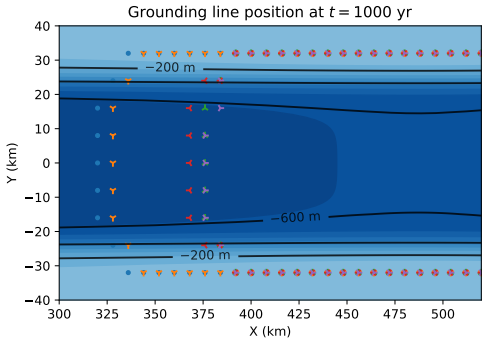

(b)

Figure 15: (a) Grounding line position of different methods inside the central flow line of the model during a 1 kyr model run. (b) The final grounding line position for the evaluated experiments at the end of the model run with bedrock elevation in metres above present day sea level given by the contour lines. Colours of the pips used in (b) match those used in figure (a).

6. Discussion

Throughout this thesis we explored the plume melt parametrisation as described by Lazeroms et al. 2019 with a extension to accommodate for two-dimensional geometries. We used for out test geometry the MISMIP+ setup which was desgined for models to be compared on their ability to simulate a retreating grounding line in a strongly buttresed enbayment area.

During testing, we found out that the default Lazeroms method of taking sixteen plume directions to construct a two-dimensional grid provided non-smooth parameter fields even on a static geometry. When we then applied the melt dynamically and allowed feedback to occur to the shelf geometry, we noticed that during the retreat the shelf geometry became irregular seeing as how sharp ice profile spikes were found close to the grounding line. We checked whether at a lower temperature forcing the melt-shelf feedback would become less noisy, but though the overall melt rate was lower, the resultant ice draft profile remained noisy.

We suggested three main avenues along which we could generate smoother parameter fields used to determine the plume-driven melt. (1) Increase the number of directions you sample plumes from. (2) Change how local slope is defined. (3) Backtrace plumes along the ice velocity field.

We showed that increasing the number of plumes did increase the smoothness of the grounding line field, but that the melt from this algorithm still caused the ice draft to become irregular and that in this setup the melt was more sustained. This effect led to what we saw in fig. 9 were the diffusive flow of ice could not smooth out the melt-driven spikes in the ice draft which was something we did observe to a lesser extent in the original algorithm at fig. 6a.

So we further adjusted this algorithm by also changing how local slope was calculated for every plume at a grid cell: instead of using down-stream gradients evaluated at a cell border, we

used central derivatives which are evaluated at the centre of a grid cell. This seemed to greatly increase the smoothness of the retreating ice draft and effectively removed spike formation during the coupled feedback simulation.

The other gradient scheme using a 'mean least squares' fit also showed that we also acquire accurate local slope gradients by way of fitting a second order polynomial surface with a 3x3 stencil at every grid point. This method also showed that this melt scheme is very sensitive to where and how you calculate your gradients. In general is seems that both central gradients and polynomial surface gradients give acceptable results but both still cause some unwanted features inside the ice draft geometry to appear as we discussed in section 5.3 and section 5.4 respectively.

We furthermore looked at the interpolation algorithm of the grounding line position. We compared Lazeroms' assumption that the grounding line position lies at the halfway point in between the last-grounded and first floating grid point to a linear interpolation algorithm that is derived from the floatation balance of ice. We determined in section 5.3.1 that switching interpolation algorithms did cause some shift in the model's response, but that this is response was minor when compared to effects of, e.g., a change in slope algorithm caused.

However using the ice velocity field to backtrace the plume origin to some point at the grounding line proved to not increase the stability of the melt feedback because the resultant ice draft contained many spikes. Also in practise the Lagrangian method was also undesirable because it is far more computationally expensive than all other methods and therefore seems to be unsuitable for larger scale setups.

7. Conclusion

In short the original Lazeroms parametrisation of a one-dimensional melt plume can be effectively implemented inside a model, but the original sixteen plume averaging procedure which Lazeroms proposed to extend the plume model to be applicable to a two-dimensional ice shelf tended in our model to lead to an unstable ice draft geometry.

The solution we had found was to, instead of just using a possible sixteen plume average, to try and trace from a given point to all valid grounding line points. We also proposed that to determine local slope we should use central gradients or a 2nd order polynomial fit to the ice draft.

These additions seemed to be quite effective at increasing the smoothness and stability of the plume-based melt model coupled to a dynamic ice draft. We would like to end of this thesis with some possible roads of inquiry wherewith this setup can be further tested and explored.

8. Outlook

While we have explored many different options and combinations of constructing valid 2D fields for the UPP melt scheme there are still many more options to explore, e.g., in determining plume properties for a grid cell we average over all valid plumes, assigning equal weight to each plume. However, the argument could be made that plume from deeper waters have more

melt potential than shallow plumes and should therefore be assigned in higher weight in the averaging procedure.

Furthermore because we have run these model setups at relatively low resolution, we not only have to contend with a grounding line that is not accurately resolved, but also the shelf geometry near the grounding line consists of only a couple of grid points. This may be problematic for applying the melt scheme near the grounding line because the melt strength is dependent on ice draft slope which is a quantity which varies significantly near this region. It would therefore be of interest to see whether higher resolution runs would significantly alter the melt patterns or effect the stability of the melt schemes

It is also important to note that we have not tried these procedures inside an Antarctic ice model, but only in a small and idealised test setup. We would therefore suggest that for better comparisons these different methods should be compared inside a full model setup to see whether the different plume schemes can lead to significant differences in ice loss.

We also saw that the gradient methods are very important in assuring the stability of the resultant melt feedback on the shelf. While we think that both central gradients as well as polynomial gradients give good results and can also be used inside a full marine ice-sheet setup, it may yet be fruitful to test whether increasing the polynomial stencil or using other gradient selection criteria would increase model stability.

In the end, we have shown that inside a simple enbayment setup we can use the parametrised form of Jenkin's melt plume model which was meant for a one-dimensional setup inside a two-dimensional environment. The modifications we proposed for acquiring grounding line depth and local slope have significantly increased the stability of the melt-shelf feedback in our model and we think that the current setup is worth exploring inside a larger marine ice-sheet model.

References

Beckmann, A and H Goosse (2003). "A parameterization of ice shelf–ocean interaction for climate models". In: *Ocean Modelling* 5.2, pp. 157–170. DOI: 10.1016/S1463-5003(02)00019-7.

Bresenham, J. E. (1965). "Algorithm for computer control of a digital plotter". In: *IBM Systems Journal* 4.1, pp. 25–30. DOI: 10.1147/sj.41.0025.

Favier, Lionel et al. (2019). "Assessment of sub-shelf melting parameterisations using the ocean–ice-sheet coupled model NEMO(v3.6)–Elmer/Ice(v8.3)". In: *Geoscientific Model Development* 12.6, pp. 2255–2283. DOI: 10.5194/gmd-12-2255-2019.

Fornberg, Bengt (31, 1988). "Generation of Finite Difference Formulas on Arbitrarily Spaced Grids". In: *Mathematica of Computation*.

Gladstone, R. M., A. J. Payne, and S. L. Cornford (2010). "Parameterising the grounding line in flow-line ice sheet models". In: *The Cryosphere* 4.4, pp. 605–619. DOI: 10.5194/tc-4-605-2010.

Gudmundsson, G. H. (2013). "Ice-shelf buttressing and the stability of marine ice sheets". In: *The Cryosphere* 7.2, pp. 647–655. DOI: 10.5194/tc-7-647-2013.

Jenkins, Adrian (1991). "A One-Dimensional Model of Ice Shelf-Ocean Interaction". In: *J. Geophys. Res.*

Lazeroms, Werner M. J. et al. (2018). "Modelling present-day basal melt rates for Antarctic ice shelves using a parametrization of buoyant meltwater plumes". In: *The Cryosphere* 12.1, pp. 49–70. DOI: 10.5194/tc-12-49-2018.

Lazeroms, Werner M. J. et al. (2019). "An Analytical Derivation of Ice-Shelf Basal Melt Based on the Dynamics of Meltwater Plumes". In: *Journal of Physical Oceanography* 49.4, pp. 917–939. DOI: 10.1175/jpo-d-18-0131.1.

Levermann, Anders et al. (2020). "Projecting Antarctica's contribution to future sea level rise from basal ice shelf melt using linear response functions of 16 ice sheet models (LARMIP-2)". In: *Earth System Dynamics* 11.1, pp. 35–76. DOI: 10.5194/esd-11-35-2020.

Oppenheimer, Michael et al. (2019). Sea Level Rise and Implications for Low-Lying Islands, Coasts and Communities. In: *Special Report on the Ocean and Cryosphere, Technical Summary*. Chap. 4.2.3.12.

Parizek, B. R. et al. (2013). "Dynamic (in)stability of Thwaites Glacier, West Antarctica". In: *Journal of Geophysical Research: Earth Surface* 118.2, pp. 638–655. DOI: 10.1002/jgrf.20044.

Pattyn, F. et al. (2012). "Results of the Marine Ice Sheet Model Intercomparison Project, MISMIP". In: *The Cryosphere* 6.3, pp. 573–588. DOI: 10.5194/tc-6-573-2012.

Pollard, D. and R. M. DeConto (2012). "Description of a hybrid ice sheet-shelf model, and application to Antarctica". In: *Geoscientific Model Development* 5.5, pp. 1273–1295. DOI: 10.5194/gmd-5-1273-2012.

Schoof, Christian (2007). "Marine ice-sheet dynamics. Part 1. The case of rapid sliding". In: *Journal of Fluid Mechanics* 573, pp. 27–55. DOI: 10.1017/s0022112006003570.

A. Constants

Symbol	Parameter Name	Value	Unit
g	Gravitational acceleration	9.81	m^2/s
E_0	Entrainment coefficient	3.6×10^{-2}	unitless
C_d	Drag coefficient	2.5×10^{-3}	unitless
λ_1	Freezing point salinity coefficient	-5.73×10^{-2}	$^\circ C$
λ_2	Freezing point offset	8.32×10^{-2}	$^\circ C$
λ_3	Freezing point depth coefficient	7.61×10^{-4}	$^\circ C m^{-1}$
$C_d^{1/2}\Gamma_T$	Thermal Stanton number	1.1×10^{-3}	unitless
$C_d^{1/2}\Gamma_S$	Haline Stanton number	3.1×10^{-5}	unitless
L	Latent heat of ice fusion	3.35×10^5	$J\ kg^{-1}$
c	Specific heat capacity of ocean water	3.974×10^3	$J\ kg^{-1}\ ^\circ C^{-1}$
c_i	Specific heat capacity of ice	2.009×10^3	$J\ kg^{-1}\ ^\circ C^{-1}$
β_S	Haline contraction coefficient	7.86×10^{-4}	unitless
β_S	Thermal expansion coefficient	3.87×10^{-5}	$^\circ C^{-1}$
C_ϵ	Slope correction parameter	0.6	unitless
ρ_i	Ice density	9.00×10^2	kg/m^3
ρ_w	Sea water density	1.00×10^3	kg/m^3
$K_{\max}$	Maximal diffusivity	5×10^{-4}	m^2/s
m	Friction law exponent	3	unitless
n	Glen's exponent	2	unitless
h_{calving}	Calving Thickness	100	m
a	Accumulation Rate	0.3	m/yr
A	Ice Rheology	6.6×10^{-24}	$s^{-1}Pa^{-3}$
β^2	Weertman Sliding Constant	7.624×10^6	$Pa\ m^{-1/3}\ s^{1/3}$
$T_{a,\text{warm}}$	Warm Ambient Ocean Temperature	-1.0	$^\circ C$
$T_{a,\text{cold}}$	Cold Ambient Ocean Temperature	-2.0	$^\circ C$
$S_{a,\text{warm}}$	Warm Ambient Ocean Salinity	34.6	PSU
$S_{a,\text{warm}}$	Cold Ambient Ocean Salinity	34.6	PSU
T_i	Ice Temperature	263.2	K

A.1. Compounds

Symbol	Expression	Value
$c_{\rho 1}$	$\frac{L/c}{C_d^{1/2}\Gamma_{TS}} \frac{\beta_T}{\beta_S S_a}$	2.0×10^2
$c_{\rho 2}$	$-\lambda_1 \beta_T / \beta_S$	2.8×10^{-3}
c_τ	$c_{\rho 2}/c_{\rho 1}$	1.4×10^{-5}

B. Bresenham Algorithm

The algorithm works by trying to best follow the standard mathematical description of a line, which is given by

$$y = ax,$$

when can write this more explicitly in that the slope is determined by the gradient of going from $y_0 \longrightarrow y_1$ over $x_0 \longrightarrow x_1$, which means that the previous statement can be written as

$$(x_1 - x_0)(y - y_0) - (y_1 - y_0)(x - x_0) = 0,$$

where $a = \mathrm{d}y/\mathrm{d}x$, $\mathrm{d}y = y_1 - y_0$ and similarly $\mathrm{d}x = x_1 - x_0$. Any error that then comes becomes of that x and y in your discretisation are not exactly on the ideal line we can write as:

$$e = \mathrm{d}x\,(y - y_0) - \mathrm{d}y\,(x - x_0).$$

Now we now that the next step is an integer step in either x, y or on the diagonal. The errors associated with each respective step are then given by:

$$\begin{aligned} e_{xy} &= (y + 1 - y_0)\mathrm{d}x - (x + 1 - x_0)\mathrm{d}y = e + \mathrm{d}x - \mathrm{d}y, \\ e_x &= (y + 1 - y_0)\mathrm{d}x - (x - x_0)\mathrm{d}y = e_{xy} + \mathrm{d}y, \\ e_y &= (y - y_0)\mathrm{d}x - (x + 1 - x_0)\mathrm{d}y = e_{xy} - \mathrm{d}x. \end{aligned}$$

We have now defined the change in error growth as interdependent variables, with the additional information that the first diagonal step produces an error of $e_{x_0+1,y_0+1} = \mathrm{d}x - \mathrm{d}y$ we can make the following line algorithm on a discretised grid:

1. Calculate e_{x_0+1,y_0+1}
2. Determine e_{xy}
3. See whether $e_{xy} + e_x > 0$, if so step in the x direction
4. See whether $e_{xy} + e_y < 0$, if so step in the y direction
5. If point $P(x_1, y_1)$ not reached, go to 2 and do the same loop for the new position

C. Mean Least Squares

The question we ask ourselves when doing a 'Mean Least Squares' (MLS) fit is how we can minimise the function

$$\min_{f \in \prod_m^d} \sum_i w\left(\mid \vec{x}_i - \vec{x}_c \mid\right) \mid f(\vec{x}_i - \vec{x}_c) - f_i \mid^2,$$

where w is a weight function only dependent on the Euclidean distance of a point $\vec{x}$ to the centre of the point where you want to apply the polynomial fit. Next f is a polynomial of degree m with d total free dimensions.In our case we want a polynomial fit which has $m = 2$ and $d = 2$, which is given by the prototypical descriptor:

$$f(x, y) = c_1 + c_2 x + c_3 y + c_4 x^2 + c_5 xy + c_6 y^2.$$

In general we can write f also as

$$f(\vec{x}) = \mathbf{b}(\vec{x})^T \mathbf{c},$$

where $\mathbf{b}(\vec{x}) = \left[b_1(\vec{x}), ..., b_k(\vec{x})\right]^T$ is the polynomial basis vector and $\mathbf{c}$ are the polynomial coefficients. For the polynomial surface we want to solve $\mathbf{b}(x, y) = \left[1, x, y, x^2, xy, y^2\right]^T$ and $\mathbf{c} = [c_1, c_2, ..., c_6]^T$.

We can obtain a general solution by solving the problem $\nabla_c E = 0$ for the error function $E = \sum_i \mid f(\vec{x}_i) - f_i \mid^2$ which decomposes to the problem where $d_i = \mid \vec{x}_i - \vec{x}_c \mid$:

$$\begin{array}{ll} \partial_{c_1} E = 0 & \sum_i 2b_1 w(d_i)(\vec{x}_i) \left[\mathbf{b}(\vec{x}_i)^T \mathbf{c} - f_i\right] = 0 \\ \partial_{c_2} E = 0 & \sum_i 2b_2 w(d_i)(\vec{x}_i) \left[\mathbf{b}(\vec{x}_i)^T \mathbf{c} - f_i\right] = 0 \\ \vdots & \\ \partial_{c_k} E = 0 & \sum_i 2b_2 w(d_i)(\vec{x}_i) \left[\mathbf{b}(\vec{x}_i)^T \mathbf{c} - f_i\right] = 0 \end{array}$$

This system of equations we can rewrite in matrix formation into:

$$\sum_i 2w(d_i)\mathbf{b}(x_i) \left[\mathbf{b}(\vec{x}_i)^T \mathbf{c} - f_i\right] = 2 \sum_i \left[w(d_i)\mathbf{b}(x_i)\mathbf{b}(\vec{x}_i)^T \mathbf{c} - w(d_i)\mathbf{b}(x_i)f_i\right] = \vec{0}$$

which we can rearrange into the following form:

$$\sum_i w(d_i)\mathbf{b}(x_i)\mathbf{b}(\vec{x}_i)^T \mathbf{c} = \sum_i w(d_i)\mathbf{b}(x_i)f_i.$$

This is solved for $\mathbf{c}$ as

$$\mathbf{c} = \left[\sum_i w(d_i)\mathbf{b}(x_i)\mathbf{b}(\vec{x}_i)^T\right]^{-1} \sum_i w(d_i)\mathbf{b}(x_i)f_i.$$

We next defined $\mathbf{A} = \sum_i w(d_i)\mathbf{b}(x_i)\mathbf{b}(\vec{x}_i)^T$. Now, because we are on a regular grid, we can make use of the fact that we only need to calculate $\mathbf{A}$ for a stencil of a given size and then the resulting matrix should hold for all points except for at the boundaries.

Finally we need a weight function. We use an exponential function in the form of

$$w(d_i) = \mathrm{e}^{-\frac{kd_i}{R}},$$

where k is a smoothing factor and R is a distance factor. For k we use a value of 8 and for the distance value we use the Euclidean distance from top left to bottom right cell corner ($R \approx 11$ km).

D. Open Data

In the interest of providing open data for others to look at, we have provided a link to an archive containing the model runs we analysed inside this thesis. `https://www.dropbox.com/s/ydhfimuzxjxwrv7/thesis.runs.meltplume.03072020.tar.xz?dl=0`